*Tribology Letters, Vol. 18, No. 4, April 2005 (© 2005)*
DOI: 10.1007/s11249-004-3597-y


# Improvement of PEEM images from thick inhomogeneous antiwear films using a thin Pt coating

M.A. Nicholls[a], G.M. Bancroft[a,*], M. Kasrai[a], P.R. Norton[a], B.H. Frazer[b] and G. De Stasio[c]

[a]*Department of Chemistry, University of Western Ontario, London, Ontario, N6A 2B7, Canada*
[b]*Syncrotron Radiation Center, University of Wisconsin–Madison, Stoughton, WI, 53589, USA*
[c]*Department of Physics, University of Wisconsin–Madison, Madison, WI, 53706-1390, USA*

Received 7 July 2004; accepted 23 December 2004

Antiwear films formed from zinc dialkyl-dithiophosphate, in base oil, are known to create inhomogeneous agglomeration of patches on metallic surfaces up to 400 nm thick. It has been found that these patches (termed antiwear pads) are also non-conducting. These two features create difficulties in analyzing data obtained using X-ray photoelectron emission microscopy (X-PEEM). Topography and near-surface charging dominate images obtained using X-PEEM techniques, which can alter electron trajectories and lower signal-to-noise counts. It has been found that the application of a *thin* continuous platinum coating provides sufficient neutralization to eliminate the positive charge-buildup and improve signal-to-noise. This improves data analysis even with the thickest pads. Examples of charging alleviation and improved signal-to-noise ratios (obtained in the P L-edge spectroscopy) are shown. Furthermore, data analysis of the spectromicroscopy stacks show improved fitting and better polyphosphate distribution mapping for the films.

**KEY WORDS:** charging, X-PEEM, Pt coating, ZDDP, antiwear, spectromicroscopy, polyphosphates, XANES, P L-edge

## 1. Introduction

The investigation of thick non-conducting films using electron spectroscopic techniques has always had its difficulties due to the charging phenomenon; poor, or lack of, conduction of electrons through a surface to replenish those leaving due to photoelectron processes. Charging typically results in diminished electron yields (signal) and can distort spectra [1–3]. Charging has also become a major obstacle in electron imaging techniques. Historically, secondary electron microscopy (SEM) was the first electron imaging technique in which charging, of non-conducting surfaces, was a problem. More recently, improvements in optics has allowed for the growth of photoelectron imaging as X-ray photoelectron spectroscopy (XPS) imaging and X-ray photoelectron emission microscopy (X-PEEM). As in SEM, charging presents a severe obstacle since spatial resolution is the defining quality of these techniques. Charging can drastically affect the imaging and spectroscopy of nearby areas since electron trajectories can be severely altered by charging regions [3]. In XPS, charging can cause distortions and large line shifts, yet its effects are much less severe for absorption measurements [3]. Typically charging is combated in two ways; (i), applying a *thin* metallic coating [4–7] or (ii) using an electron flood gun [2,8–10].

*To whom correspondence should be addressed.
E-mail: gmbancro@uwo.ca

Recent work using X-PEEM to investigate the spatially resolved microchemistry found in antiwear films, formed on metallic surfaces from phosphorus based additives in engine oil, was more difficult due to surface charging [3,11,12]. It is widely accepted that engine oil additives breakdown in a combustion engine to create reaction products that, under high temperature and pressure, create sacrificial films that are responsible for minimizing asperity contact (wear) [13]. The most common, and the best antiwear additive used in engine oils today is zinc dialkyl-dithiophosphates (ZDDPs; figure 1). Extensive reviews of its formation, composition, and performance can be found in references [14–18]. The antiwear film is formed of an agglomeration of patches (termed antiwear pads) that are raised from the surface by up to 400 nm. These large pads are responsible for limiting the contact between the two rubbing surfaces and impeding wear. Understanding the chemical [12,19–21] and mechanical [22–25] characteristics of the antiwear pads has helped to provide evidence as to how and why they work so well.

The non-homogeneous antiwear films pose two problems in electron imaging: first the heterogeneity and roughness of the surface; and second, the charging phenomenon experienced due to the non-conducting nature of the antiwear film. The challenge of this work [12,22] was to develop data analysis techniques that emphasized the chemical (X-ray absorption) information while simultaneously de-emphasizing the other contrast factors such as topography and charging. We now describe how the application of a 10-Å conductive

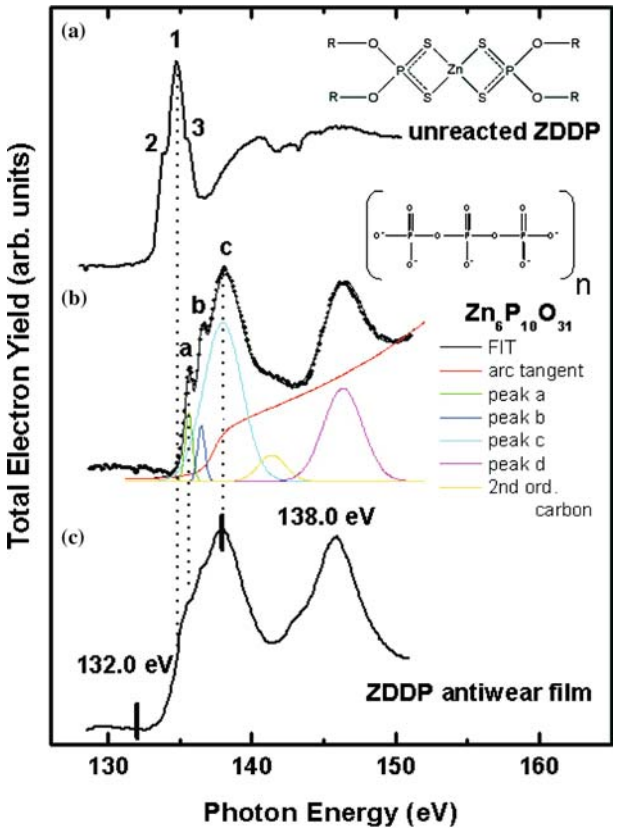


Figure 1. The P L-edge spectra obtained for unreacted ZDDP (a), a model zinc polyphosphate (b), and a ZDDP antiwear film (c). Structures for ZDDP and a polyphosphate are depicted. Also shown is an example of the peak fitting, used to determine the relative peak heights of peaks *a, b*, and *c*. Changes in the near edge structure reveal detailed information about the geometry and oxidation state of phosphorus in the film. Peak assignments are given in the text. A colored version of this figure can be found in the PDF version of this document.

platinum coating, allows for a more thorough chemical analysis of all the antiwear pads, generated from ZDDP additives on steel surfaces, at the nanometer scale.

## 2. Experimental

### 2.1. Sample preparation

The steel samples were manufactured from 52100 steel into square specimens $10 \times 10 \times 4$ mm$^3$. The composition of 52100 steel is ~1% C, 1.3–1.6 Cr and the remainder being primarily iron. The sample was polished with 3 $\mu$m diamond paste. The reciprocating cylinders were manufactured from 52100 steel with 6 mm diameter and 6 mm length. The steel sample and pins were austenitized and quenched, and their hardness was >60 Rockwell C. The pins were used as is. The samples were then washed in hexane and methanol in a ultrasonic bath for a minimum of 15 min in each.

The ZDDP antiwear films were formed in a reciprocating Plint wear tester under boundary lubrication conditions with a cylinder-on-flat test geometry establishing a line contact [12]. The test condition consisted of a rubbing time of 1 h, at 100 °C, with an applied load of 220 N, and a frequency of 25 Hz under a fully flooded state. A ZDDP commercial-concentrate was obtained from Imperial Oil, Canada. The concentrate is a mixture of neutral and basic forms, consisting of 85% secondary (C-4) and 15% primary (C-8) alkyls. The concentrate was diluted using MCT-10 base oil to 1.2 mass percent resulting in a phosphorus content of ~0.1% by weight. A grid composed of indent marks was created using a Vickers hardness tester using loads of 100 and 500 g which made indents ~25 and ~150 $\mu$m across, respectively. This grid allowed for relocation of the same regions with the multiple techniques discussed below.

### 2.2. Surface imaging

Topographical imaging was performed using a Digital Instruments Nanoscope IIIa®atomic force microscope. Images were used to investigate the morphology and topography of the antiwear films.

### 2.3. X-ray absorption near edge structure analysis (XANES)

Photoabsorption spectra were collected at the Canadian Synchrotron Radiation Facility (CSRF) Grasshopper beamline situated on the 1 GeV Aladdin storage ring, University of Wisconsin, Madison. Details of the beamline can be found elsewhere [12,26,27]. At least two individual scans were recorded, in total electron yield (TEY) mode, for each specimen and digitally combined. The spectra were normalized against $I_o$ and a linear background was subtracted. Spectra were calibrated and normalized using the BAN data analysis program [28]. The spectra are recorded from areas covered by an X-ray spot size (~6 mm$^2$), and thus give an overall average spectrum for the antiwear film.

### 2.4. X-ray photoelectron emission microscopy (X-PEEM)

Conventional photoelectron emission microscopes (PEEM) utilize UV light as the excitation source. Only recently has the coupling with synchrotron light sources, allowed for rapid advancements in both acquisition time and spatial resolution. X-ray spectromicroscopy can now provide spatially resolved analysis at the <100 nm length scales [29–32]. This has caused a dramatic increase in the potential applications for PEEM that include polymers [29], minerals [33], magnetism [34], and biological samples [35,36] to name only a few. Essentially, X-PEEM is spatially resolved XANES performed through imaging. X-rays are scanned through an

energy range onto a sample at grazing angles (typically 15–30°). Collection of the spatially orientated low energy electrons from the surface, results in electron microscopy images. The spatial distribution of emitted electrons is maintained by the use of a large electric field (20 keV) between the sample and the first aperture. A combination of stigmators, deflectors, and magnetic lenses focus and magnify the secondary electron image. This image is projected onto a multichannel plate and phosphor screen assembly where each image (at each eV step) is recorded by a 12 bit digital camera to create a secondary electron image. Grayscale coding in the image indicates intensity of signal. Image intensity in X-PEEM is similar to the XANES TEY, and surface sensitivity of the instrument is limited by the escape depth of the secondary electrons at the P L-edge (~2–10 nm) [37–39]. Sequences of images are acquired at particular step sizes (0.1 eV). These are combined to produce a three-dimensional data set or spectromicroscopy "stack" [31], which is analyzed to extract detailed elemental, chemical and topographical information about the nature of a surface at high spatial resolution. Typical areas analyzed were, on average, several hundred $nm^2$ to a few $\mu m^2$. This contrasts the ~6 $mm^2$ analysis areas using the conventional TEY method described in Section 2.3.

X-PEEM was performed using the Spectromicroscope for PHotoelectron Imaging of Nanostructures with X-rays (SPHINX microscope; ELMITEC GmbH) [40] installed on the 6 m-TGM (Toroidal Grating Monochromator) beamline at the 1 GeV Aladdin storage ring, University of Wisconsin, Madison. Details of the beamline and X-PEEM data analysis can be found in references [12,22]. XANES spectra are extracted from the spectromicroscopy stack using software [30,41] that allows for selection of a single pixel, or regions of several pixels in size. The spectra resulting from the selected regions are an average spectrum over all the pixels contained in the region. Thus some spectra are the average of a few pixels, or of several tens to hundreds of pixels yielding better signal-to-noise spectra. The software also employs advanced regression analysis procedures [30,41,42] to allow for mapping of chemical species in the film which is described elsewhere [12,22]. Essentially, model spectra are input into the regression analysis and a weight factor is applied to each model spectrum as they are compared to the spectrum extracted at each pixel in the spectromicroscopy "stack". A better fit implies a closer match to the model spectra.

After initial spectra were obtained on the Grasshopper beamline and the X-PEEM, the samples were coated with 10-Å of Pt (99.99% purity; Ted Pella Inc, CA) by magnetron sputtering (Cressington, UK) at room temperature, in $1.5 \times 10^{-2}$ Torr Ar, and with a 40 mA current. The samples were rotated while being sputter coated to create an even, continuous coating across the non-homogeneous antiwear film. The thickness of the Pt coating was monitored by a quartz crystal thickness monitor, which has a thickness sensitivity of 0.1-Å. Samples were run again in the Grasshopper monochromator beamline [27], and then run in the SPHINX microscope (Elmitec, GmbH).

## 3. Results and discussion

### 3.1. Analysis of thin (<350 nm) antiwear films

Analysis of the X-PEEM data collected from ZDDP antiwear films, formed on steel surfaces, proved to have its difficulties [3,11,12]. X-PEEM images (photoelectron images) of the ZDDP antiwear films were dominated by topography, charging effects, variable sampling depth, work function, and shadowing. Due to previous analysis of antiwear films by scanning probe microscopy [12,23,43–45], it is well known that topography would be the primary contrast feature in our photoelectron images (PI). In order to understand fully the PIs obtained from the samples, a grid system created by macro-scale indents was used for re-location of the same areas, and hence features, with atomic force microscopy (AFM) and X-PEEM.

X-ray absorption spectroscopy (XAS) has shown that ZDDP antiwear films are formed of a bilayer structure in which shorter-chain polyphosphates are found at the metal-film interface and long-chain polyphosphates are found at the surface [12,46]. This can be determined using phosphorus L-edge X-ray absorption near edge structure (XANES) analysis with total electron yield (TEY) detection for the surface and fluorescence yield (FY) detection for the bulk. It has been determined that the near-edge fine structure at the P L-edge is very sensitive to small changes in the oxidation and local chemical environment around the absorbing phosphorus atom [46,47]. XANES analysis at the P L-edge probes transitions from occupied 2p orbitals to unoccupied antibonding orbitals. Figure 1 shows the P L-edge spectra obtained from unreacted ZDDP (spectrum (a), a model zinc polyphosphate ($Zn_6P_{10}O_{31}$; spectrum (b), and that obtained from a ZDDP antiwear film (spectrum (c)). At the P L-edge three distinct peaks can be observed (see figure 1). The first two peaks on the lower energy side of the phosphorus L-edge spectrum, denoted as *a* and *b* in figure 1, are assigned to the transitions of electrons from the core $2p_{3/2}$ and $2p_{1/2}$ levels (spin-orbit split by 0.88 eV) to the $a_1^*$ anti-bonding orbital. Peak *c* is attributed to the transition of the 2p electrons to a p-like molecular orbital. Peaks *a, b*, and *c* in the spectra of the polyphosphate and the antiwear film indicate that the local chemical environment around the P atom has changed. These peaks are shifted to higher energy compared with peaks 1, 2, and 3 characteristic of unreacted ZDDP. It can be inferred from the presence of peaks *a, b*, and *c* in the spectrum of the antiwear film, that the film has a zinc polyphosphate structure. The spectra were fitted using the BGauss

multiline fitting program version 2.3 [48]. An example fit for the $Zn_6P_{10}O_{31}$ glass is shown in figure 1. An arc tangent background was positioned at the absorption edge for phosphorus. Peaks *a, b*, *c*, and *d* were fitted using Gaussian peaks. Peaks *a* and *b* were fixed to be equal in width and to have a splitting of 0.88 eV. A Gaussian peak at ~142.5 eV was used to improve the fit and positioned for second-order carbon contamination of the beamline optics. The resulting fit values were used to investigate the relative peak height ratio to the number of P-atoms in the polyphosphate chains [12,49,50].

Previous results have shown that X-PEEM can be successfully used to image, and perform chemical analysis, of polyphosphates found in ZDDP antiwear films [11,12,22]. The selection, and analysis, of regions of the antiwear films had to be done with extreme care. In our previous reports, charging was a problem [11,12, 22] and only areas which provided interpretable results were used. This required careful selection of areas that contained pads of < 300 nm thickness that did not charge excessively. Areas that had significant charging complicated the analysis and often provided results that were difficult to interpret (see below).

Figure 2(a) shows an AFM image of an area, which contains some large antiwear pads. The image also contains a region between the pads, which contains smaller pads and presumably decomposition intermediates. This area is similar to those previously analyzed [12,22] and have provided decent results even when charging was a problem. The antiwear pads are elongated in the direction of rubbing. Corresponding PIs are shown in (b) and (c). Image (b) is taken at 132.0 eV (below the peak) and image (c) is taken at 138.0 eV (on the peak, see figure 1 spectrum (c) for energy locations). These images correspond to the phosphorus pre-edge, and L-edge maximum of polyphosphate. Bright areas in a PI are due to a high electron yield from the surface, and darker areas are due to a suppression of electron signal by the charging nature of the non-conducting antiwear film. It can be observed in figure 2(b) and (c) that the larger antiwear pads are charging and appear dark due to the suppression of electron signal from the surface. Charging is typical in thick non-conducting films that result in a build-up of positive near-surface electrical charge, which is not compensated for by electron conduction through the film. This charging yields poor signal, distortions in the electron images [3,51], and even the creation of negative peaks in spectra [3]. Some of these effects have been observed previously on ZDDP antiwear films [11,12] and on other non-conducting samples [3,33,51] using X-PEEM.

Based on the principles of PEEM, images taken before an absorption edge should lack any secondary electron signal due to the relaxation processes after the P L-edge absorption, and thus be primarily dominated by topography and shadowing (in the case of rough surfaces such as antiwear films; PEEM is ideal on relatively featureless surfaces). At the P L-edge the signal intensity in the images is a combination of both topography and secondary electrons due to the relaxation processes. A common method of removing topography from an image is by making a ratio image between the pre-edge (figure 2(b)) and edge maximum image (figure 2(c))[11,33,52]. A ratio image, of image (c) divided by image (b) (from here on referred to as a difference image, or image (c)/image (b)), is shown in figure 2(d). Bright areas in the difference image are primarily due to an increase in electron signal from areas containing phosphorus, and dark areas are due to little or no phosphorus signal. It can be observed that the strong phosphorus signal in the image is distributed non-uniformly across the film, and corresponds approximately to the AFM image in figure 2(a).

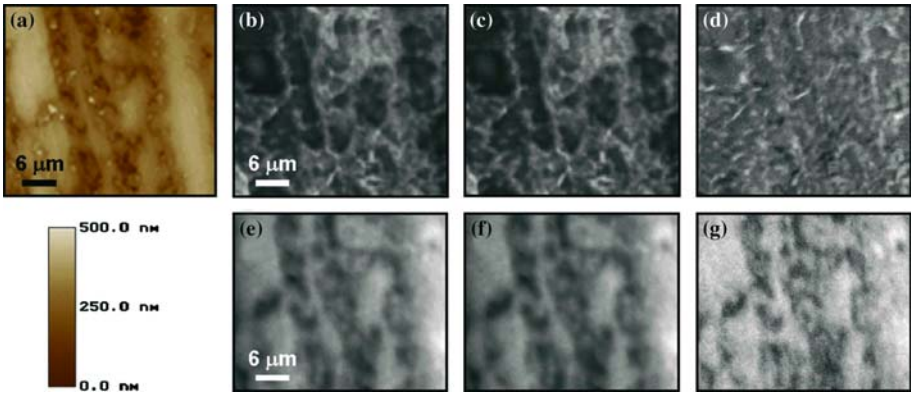


Figure 2. An AFM topography image is shown of a ZDDP antiwear film (a) with features ( < 350 nm in height). A height scale is provided below the image. The long patches are termed antiwear pads. Images (b)–(d) are for the non-coated film and images (e)–(g) are for the Pt coated film. Images (b) and (e) are taken at 132.0 eV of the corresponding AFM region. Images (c) and (f) are taken at 138.0 eV of the same AFM region. In images (b) and (c) the thick non-conducting pads charge and results in a suppression of the electron signal and appear black. The Pt coating alleviates the charging phenomenon. Image (d) is a difference image of image (c) divided by image (b) (image (c)/image (b)) and image (g) is a difference image of image (f)/image (e). A colored version of this figure can be found in the PDF version of this document.

In SEM the application of a *thin* metal film is used to overcome the charging problem [4,6,7,51,53]. This technique has also been applied to combat charging in X-PEEM [3,33,51]. Thus in order to improve the X-PEEM imaging technique on the non-homogeneous ZDDP antiwear films, a thin 10-Å platinum coating was sputter coated onto the antiwear film. Figure 2(e) and (F) are the PIs as a result of the Pt coating. Figure 2(e) was acquired at 132.0 eV and figure 2(f) is taken at 138.0 eV. These images are of the same area and correspond to the charged figure 2(b) and (c), respectively. It can be observed that the Pt coating has alleviated the charging problem by allowing for an even conduction of electrons across the surface of the film. The SPHINX microscope makes use of a −20 kV potential that is applied to the sample to aid in the electron collection process (the first aperture is at ground potential) [40]. Due to the inhomogeneous nature of the antiwear film there are likely areas where the Pt coating is making electrical contact to the biased substrate and flooding the surface with charge-compensating electrons. In figure 2(e) and (f) the large (formerly non-conducting) antiwear pads are now clearly visible as bright areas in the images, indicating that good electron signal is being collected from the surfaces of the pads. As was mentioned above (for this particular condition) the large signal is a result of both topography and chemical excitation. A difference image between image (f)/image (e), removes the signal that is primarily due to topography, and is shown in figure 2(g). Thus the image shows the areas that are emitting a large electron signal due to phosphorus absorption (at peak *c*) and resultant relaxation processes. Hence, these areas are composed of polyphosphates. Comparison of image (g) to image (a) shows a much better correlation between the antiwear pad height and the polyphosphate signal, than for the uncoated sample in figure 2(d). Areas between the pads have a lower polyphosphate signal. From these results it is very evident that the 10-Å Pt coating is very useful in removing the charging problem associated with the thick inhomogeneous antiwear film. The removal of the charging allows for better distinction between chemical and topographical changes in the film.

As was mentioned, above work by Yin *et al*. [46] has shown that long-chain and short-chain polyphosphates can be characterized by differences in the ratios of peaks *a:c* (see figure 1(b)), where a large ratio ( > 0.5) indicates a long-chain, and a small ratio ( < 0.5) is for shorter-chain polyphosphates. In our previous studies we have been able to identify long- and short-chain polyphosphates at the surface of the film [11,12,22].

The X-PEEM analysis has further allowed for chemical mapping of long- and shorter-chain polyphosphates in the film. Large pads had long-chain polyphosphates at their surface and shorter-chain polyphosphates were found in the valleys between the pads. Such an analysis is shown in figures 3(a)–(c). In the film prior to Pt coating (figure 2(a) and (b)), long- and short-chain polyphosphates were found (two spectra exhibiting significantly different polyphosphate chain-lengths with a good signal-to-noise ratio). These spectra are classified as internal model spectra (see figure 3(g), spectra 1 and 2) which allows for the most accurate mapping when regions of pure material cannot be identified in an area [42]. Maps of the long- and shorter-chain polyphosphates were obtained by analyzing the image sequence from the P L-edge stack. Analysis using the entire spectromicroscopy stack (all of the images) allows the full P L-edge region to be used in deriving spatial distributions (maps) of the components.

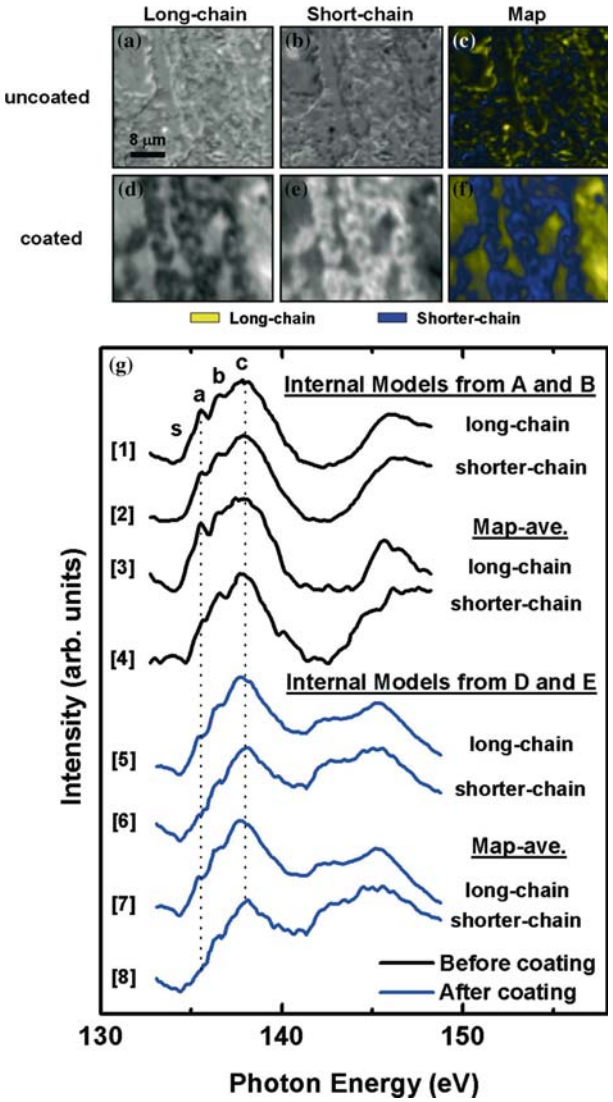


Figure 3. Images (a) and (d) are the long-chain polyphosphate maps for the film before (charging) and after the film was coated with 10-Å of Pt (non-charging). Images (b) and (e) are the short-chain polyphosphate maps, respectively. Images (c) and (f) are the combined polyphosphate distribution maps for the sample before and after Pt coating. The internal model spectra and map average spectra obtained from the film before and after coating, are shown in (g). Description of the spectra can be found in the text. A colored version of this figure can be found in the PDF version of this document.

A pixel-by-pixel linear regression procedure, using the singular value decomposition (SVD) technique [42], was used to derive the component maps shown in figure 3(a) and figure 3(b) for the charged film.

Figure 3(a) and (b) are the single component maps for the long- and short-chain polyphosphate maps prior to Pt coating, respectively. Brightness in the image indicates an abundance of the corresponding polyphosphate species. The component maps were then digitally combined to produce a polyphosphate distribution map (see figure 3(c)). Yellow in the image shows the location of the long-chain polyphosphates and blue indicates the location of shorter-chain polyphosphates. A signal mask was generated for each of the components and corresponding spectra were extracted (from multiple pixels within each mask). These map-average spectra are shown in figure 3(g), spectra 3 and 4, and are used to confirm the fitting procedure. It can be seen that the map-average spectra for the long- and shorter-chain polyphosphates very closely resemble that of their internal model spectra, thus confirming the accuracy of the mapping procedure. It can also be observed in the polyphosphate distribution map that the long-chain polyphosphates seem to be located in the vicinity of the edges of the antiwear pads and that shorter-chain polyphosphates are located between the pads.

The same procedure was performed after the 10-Å Pt coating was sputtered onto the film. The results are shown in figure 3(d)–(f). It can be observed that much better fits (a better fit implies a closer match to the model spectra) were obtained for the film once the signal-to-noise ratio was improved. Figure 3(d) and (e) show a much better resolved location for the long- and shorter-chain polyphosphates. As a result of the better single component maps, a much cleaner distribution map was obtained (figure 3(f)). The internal model spectra used for the mapping of the Pt coated film are shown in figure 3(g), spectra 5 and 6. Also, the map-average spectra obtained from the masks of the Pt coated film are also shown (spectra 7 and 8). It can be observed that the map-average spectra are almost identical to the internal model spectra, confirming the accuracy of the mapping procedure, and thus a better fit due to the reduction in the charging. The differences observed between figure 3(c) and (f) are due to the slight charging of the antiwear pads. In figure 3(c) the charging has distorted the trajectories of the electrons leaving the surface, placing the long-chain polyphosphate signal at the edges of the antiwear pads.

### 3.2. Analysis of thick (>350 nm) antiwear films

Figure 4(a) shows an AFM topography image of an area of a ZDDP antiwear film that has severe charging due to thicker (>350 nm) antiwear pads. At the bottom-center of the image, the corner of one of the square grid marks can be observed. This example emphasizes the care that must be taken when choosing an area for analysis. Areas which have significant charging (due to thick pads) produce results that are difficult to interpret. The corresponding PI images, of the AFM image, are shown in (b) and (c). Image (b) is taken at 132.0 eV and image (c) is taken at 138.0 eV, corresponding to the phosphorus pre-edge, and L-edge. The difference image [11,33,52] (image (c)/image (b)) is shown in figure 4(d). It can be observed that very little phosphorus signal can be observed in the image, and a slightly higher signal can be found in the areas around and between the large antiwear pads (in comparison to image (a)). This is in slight contrast to what was observed earlier for the region with thinner (less charging) antiwear pads.

Figure 4(e) and (f) are the PIs as a result of the Pt coating. Figure 4(e) was acquired at 132.0 eV (pre-peak) and image F is taken at 138.0 eV (at peak *c*). Again, it can be observed that the Pt coating has alleviated the charging problem by allowing for an even conduction of electrons across the surface of the film. In images (e) and (f) the large (formerly non-conducting) antiwear pads are now clearly visible as bright areas in the images, indicating that good electron signal is being collected from the surfaces of the pads. As was mentioned above the large signal is a result of both topography and chemical excitation. The difference image (image (f)/image (e)), which removes topography, is shown in figure 4(g). Thus figure 4(g) shows the areas that are emitting a large electron signal due to phosphorus absorption (at peak *c*) and resultant relaxation. It can be observed that areas between the pads have a lower polyphosphate signal than the pads themselves.

The benefits of the relatively uniform charge compensating potential, across the surface, can also be identified as a drastic improvement in the signal-to-noise ratio in the spectra (the effects of which will be described below). Figure 5(a) and (b) are magnified images of figure 4(c) and (f), of the large elongated antiwear pad at the left of the image, for the sample before coating (charging) and after (non-charging), respectively. The X-PEEM analysis software [30,41] allows for extraction of spectra from a single pixel, or gives an average spectrum over all the pixels contained in a selected region. Spectra were extracted from the areas outlined as 1, 2, and 3 in figure 5(a) (top spectra) and figure 5(b) (bottom spectra). Due to the charging, a poor signal-to-noise ratio was obtained for the spectra and fine structure was difficult to observe. However after sputter coating the film with 10-Å of Pt, the charging was eliminated and spectra extracted from the same areas had a much better signal-to-noise ratio (see figure 5(c), bottom spectra). Thus the Pt coating had two very important advantages for the analysis of data from inhomogeneous, non-conducting antiwear films, (i) it helped remove topography from the images and allowed for better identification of chemical changes in the film,

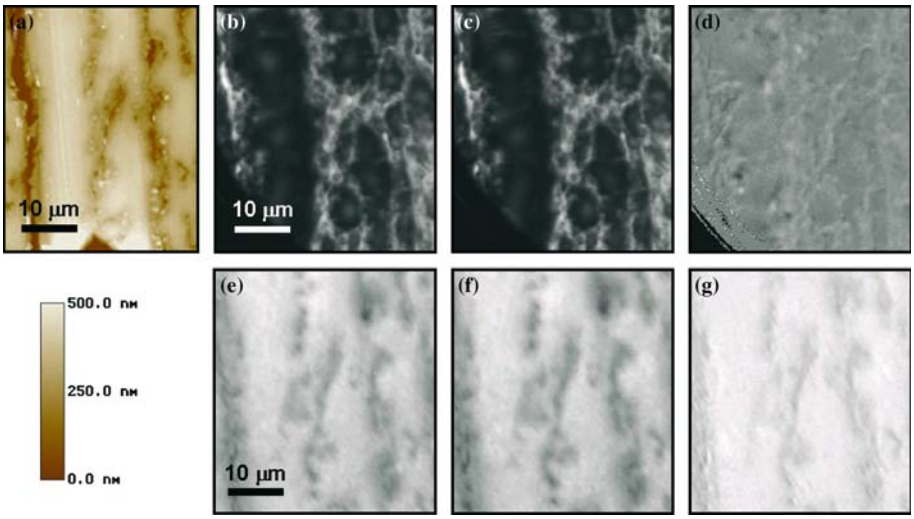


Figure 4. An AFM topography image is shown of a ZDDP antiwear film (a) with features ( > 350 nm in height). A height scale is provided below the image. The long patches are termed antiwear pads. Images (b)–(d) are for the non-coated film and images (e)–(g) are for the Pt coated film. Images (b) and (e) are taken at 132.0 eV of the corresponding AFM region. Images (c) and (f) are taken at 138.0 eV of the same AFM region. In images (b) and (c) the thick non-conducting pads charge and results in a suppression of the electron signal and appear black. The Pt coating alleviates the charging phenomenon. Image (d) is a difference image of image (c)/image (b) and image (g) is a difference image of image (f)/image (e). A colored version of this figure can be found in the PDF version of this document.

and (ii) the larger signal-to-noise ratio allowed for the fine structure in the P L-edge spectra to be observed much more obviously on the formerly charging antiwear pads.

The poor signal-to-noise ratio in the spectra also created difficulties in the mapping of the polyphosphate distribution in the charging films. As was performed above for the *good* area (area which did not have a substantial amount of charging), two spectra exhibiting significantly different polyphosphate chain-lengths with *good* signal-to-noise ratios were extracted from the spectromicroscopy stack. The spectra are shown in figure 6(g), spectrum 1 and 2. Figure 6(a) and (b) are the single component maps for the long- and short-chain polyphosphates in the charging film, respectively. Figure 6(c) shows the polyphosphate distribution map. Yellow in the image shows the location of the long-chain polyphosphates and blue indicates the location of shorter-chain polyphosphates. It can be observed the distribution map is very mottled and a direct correlation between the antiwear pads and polyphosphates is difficult to make. The map-average spectra are shown in figure 6(g), spectra 3 and 4 and are used to confirm the fitting procedure. It can be seen that the map-average spectrum for the long-chain polyphosphate very closely resembles that of the internal model spectra. However the shorter-chain polyphosphate spectrum has a poor resemblance to the original map average spectrum. This is unlike the previous example (in which the film was thinner and the charging was not as drastic). This demonstrates a weakness in the analysis, which is a result of the significant charging, resultant poor signal-to-noise ratio in the spectra, making the fitting less accurate.

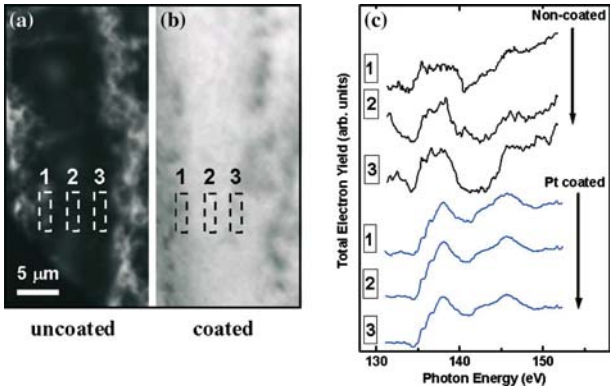


Figure 5. Images (a) and (b) are a magnified view of the large antiwear pad observed in figure 4. Image (a) is for the sample before coating and image (b) is after the film was Pt-coated. Spectra are extracted from the spectromicroscopy stack in the regions shown (1–3) from each of the stacks (shown in (c)). It can be observed from the spectra that a much better signal-to-noise ratio is obtained from the film after it has been Pt coated.

After the Pt coating was sputtered onto the film, much better fits were obtained for the film (since the signal-to-noise ratio was improved) and figure 6(d) and (e) show a much better resolved location of the long- and shorter-chain polyphosphates. As a result of the better single component maps, a much cleaner distribution map was obtained (figure 6(f)). The internal model spectra used for the mapping of the Pt coated film are shown in figure 6(g), spectra 5 and 6. Also, the map-average spectra obtained from the masks of the Pt coated film are also shown (spectra 7 and 8). Again, it

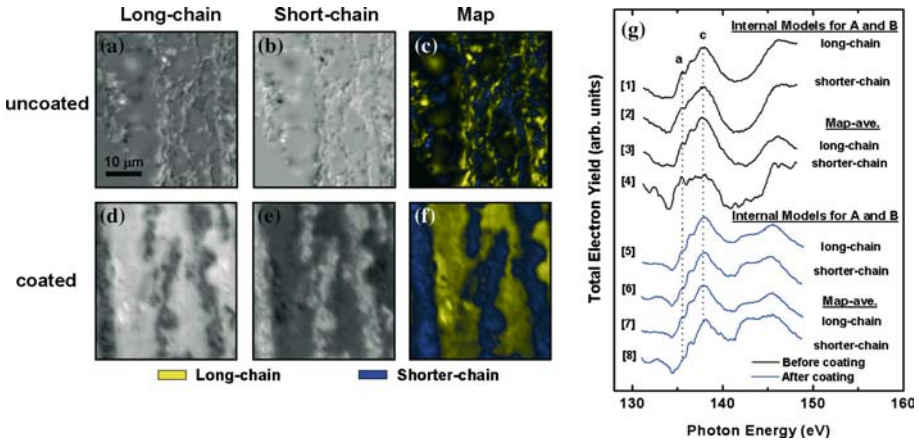


Figure 6. Images (a) and (d) are the long-chain polyphosphate maps for the film before (charging) and after the film was coated with 10-Å of Pt (non-charging). Images (b) and (e) are the short-chain polyphosphate maps respectively. Images (c) and (f) are the combined polyphosphate distribution maps for the sample before and after coating, respectively. The internal model spectra and map average spectra obtained from the film before and after coating, are shown in (g). Description of the spectra can be found in the text. A colored version of this figure can be found in the PDF version of this document.

can be observed that the map-average spectra area almost identical to the internal model spectra confirming the accuracy of the mapping procedure, and a better fit due to the reduction in the charging by the Pt coating.

### 3.3. Other effects of the Pt coating

An interesting effect was observed when the *a:c* ratios of the spectra, obtained from the sample before and after Pt-coating, of long- and short-chain polyphosphates were compared. It was found that, for the long-chain polyphosphate spectra, the sample before coating had an *a:c* ratio that was larger than the Pt coated long-chain polyphosphate spectra (see below). This led us to examine two theories, (i) that the sputtered film was chemically reacting with the long-chain polyphosphate film to create shorter-chain polyphosphates or, (ii) that there was a change in the detection mode of the SPHINX microscope. We ruled out the first mechanism since the Pt should be near room temperature when it hit the surface and should not thermally decompose the film or react with long-chain polyphosphates to give short-chain polyphosphates. We thus performed a deeper investigation into the second theory.

As was previously observed, a ZDDP antiwear film formed from ZDDP in base oil, under tribological conditions, formed a bilayer polyphosphate film [12,46]. In figure 7, the grasshopper data are acquired from of spot size ~6 $mm^2$ and thus give a global average of the entire film. The Grasshopper spectra taken before (spectrum (a)) and after (spectrum (b)) the antiwear film was coated are shown. Spectra (c) and (d) are obtained from the X-PEEM before and after coating with Pt. A measure of the relative peak height ratios of peaks *a:c* give peak height ratios of 0.62 for both spectrum acquired with the Grasshopper. This ratio is indicative of a

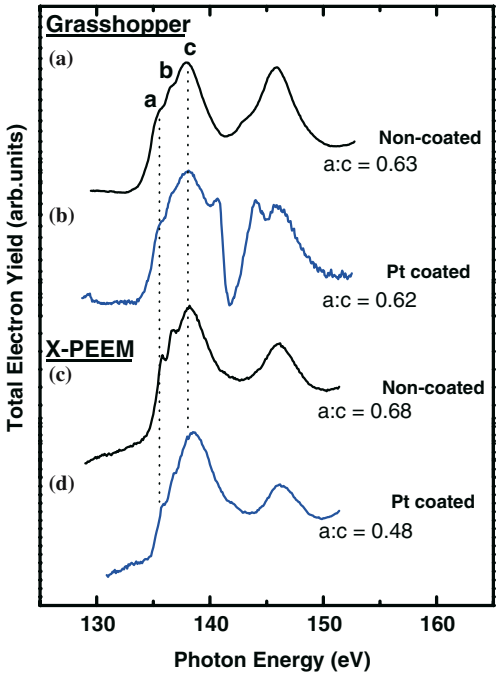


Figure 7. The P L-edge spectra of the sample taken with the Grasshopper before coating (spectrum (a)) and after coating with Pt (spectrum (b)). The spectra taken of the antiwear film using the SPHINX microscope before coating is shown (c) and after coating (d). Also listed are the relative peak height ratios for peaks *a:c*, which are a semi-quantitative measure of the polyphosphate chain length (see text).

long-chain polyphosphate [12,46]. The large dip observed at ~140 eV in spectrum B is due to carbon contamination of the beamline optics. Two small peaks have previously been observed at ~142 eV that is due to the high second order carbon signal (285 eV/2 –142 eV) from the grating of the Grasshopper beamline which transmits substantial second order radiation [22,45]. This can appear as a dip if the sample signal is weak compared to the carbon absorption.

X-PEEM spectra (c) and (d) are obtained from the same sample and give micro-scale analysis ($\sim$400 $\mu m^2$) compared to that of the Grasshopper beam spot. It can be observed that after the application of the Pt coating the *a:c* ratio drastically drops from 0.68 to 0.48. A difference of $\sim$0.2 in the relative peak height ratios measured is significant and suggests a difference of 5–10 phosphorus atoms in the chain length [12] of the polyphosphate detected at the surface of the film. This is an indication that the Pt coating could possibly be increasing the escape depth and allowing for a more bulk measurement, *similar* to the Grasshopper florescence yield measurements in previous publications [12,46]. This can be qualitatively rationalized using classical electrostatic principles and solid-state physics. In X-PEEM a large negative voltage is applied to the sample that is used to establish an electric field between the sample and the electrically grounded first aperture. The electric field aids in the collection of the low kinetic energy secondary, and Auger electrons, escaping the surface and maintaining their spatial orientation [40]. It is believed that the combination of the Pt coating, and the large negative voltage applied to the sample, is responsible for creating a stronger electric field extracting electrons from the sample bulk to the surface and then to the microscope optics column. This results in a more bulk analysis technique giving electrons a larger mean free path. To investigate this phenomenon further we have analyzed silicon samples with different anodically grown oxide thicknesses (between 10 and 317 Å) before and after the application of a 10-Å Pt sputter coating using the Grasshopper and SPHINX microscope. We have found that the sample bias improves depth sensitivity, but also the Pt coating enhances the process. This was semi-quantified as an increase of $\sim$100% and will appear in a future publication [54].

## 4. Conclusions

It has been found that the inhomogeneous, nonconducting nature of the ZDDP antiwear films pose severe obstacles when analyzing the spectromicroscopy stacks obtained by X-ray photoelectron emission microscopy (X-PEEM). The challenge of this work was to develop data analysis techniques that emphasized the chemical (X-ray absorption) information while simultaneously de-emphasizing the other contrast factors such as topography and charging. The primary contrast feature in X-PEEM images of heterogeneous (rough) surfaces is topography. In the case of ZDDP antiwear films, charging of the thick antiwear pads was responsible for distorting the image and producing a poor signal-to-noise ratio in the extracted P L-edge spectra. It was found that the application of a thin 10-Å continuous Pt coating on the antiwear film was sufficient to reduce the charging and improve the analysis of the antiwear films. The Pt-coating was responsible for compensating the extra positive charge generated on the large antiwear pads, and improved the signal-to-noise ratio in the spectra and helped to improve the fitting procedure used to create the polyphosphate distribution maps.

An unusual effect was observed between the spectra before coating and after coating with Pt. It was found the relative escape depth of the low energy electrons appears to have increased after the application of a 10-Å Pt coating, particularly in the SPHINX microscope, making it more bulk sensitive. This will be further explored in an upcoming publication [54].

## Acknowledgments

M.A.N would like to personally thank A.P. Hitchcock for his help with aXis2000 and useful discussions about the analysis of the X-PEEM data. The authors would also like to thank K. Tan, A. Jurgensen, and the staff of the Synchrotron Radiation Center (SRC), University of Wisconsin, Madison, for their technical support. We are grateful to the National Science Foundation for supporting the SRC under Award # DMR-00-84402. Financial support was provided by General Motors of Canada Ltd., and Natural Sciences and Engineering Research Council of Canada.

## References

[1] D.R. Baer, M.H. Engelhard, D.J. Gaspar, A.S. Lea and C.F. Windisch, Surf. Interface Anal. 33 (2002) 781.
[2] T.L. Barr, J. Vac. Sci. Tech. A 7 (1989) 1677.
[3] B. Gilbert, R. Andres, P. Perfetti, G. Margaritondo, G. Rempfer and G. De Stasio, Ultramicroscopy 83 (2000) 129.
[4] J.I. Goldstein, H. Yankowitz, D.E. Newbury, E. Lifshin, J.W. Colby and J.R. Coleman, *Practical Scanning Electron Microscopy: Electron and Ion Microprobe Analysis* (Plenum Press, London, 1975).
[5] M.A. Hayat, *Principles and Techniques of Scanning Electron Microscopy: Bilogical Applications* 4(Van Nostrand Reinhold Company, London, 1975).
[6] C.E. Lyman, J.I. Goldstein, A.D. Romig, P. Echlin, D.C. Joy, D.E. Newbury, D.B. Williams, J.T. Armstrong, C.E. Fiori, E. Lifshin and K.-R. Peters, *Scanning Electron Microscopy, X-ray Microanalysis, and Analytical Electron Microscopy: A Laboratory Workbook* (Plenum Press, New York, 1999).
[7] G.T. Belz and G.J. Auchterlonie, Micron 26 (1995) 141.
[8] H.W. Nesbitt, G.M. Bancroft, R. Davidson, N.S. McIntyre and A.R. Pratt, Am. Mineral. 89 (2004) 878.
[9] G. Vereecke and P.G. Rouxhet, Surf. Interface Anal. 26 (1998) 490.
[10] T. Tanaka, K.K. Bando, N. Matsubayashi, M. Imamura H. Shimada, J. Elect. Spectro. Rel. Phen. 114–116 (2001) 1077.
[11] G.W. Canning, M.L. Fuller, G.M. Bancroft, M. Kasrai, J.N. Cutler, G. De Stasio and B. Gilbert, Tribol. Lett. 6 (1999) 159.
[12] M.A. Nicholls, P.R. Norton, G.M. Bancroft, M. Kasrai, T. Do, B.H. Frazer and G. De Stasio, Tribol. Lett. 17 (2004) 205.
[13] I.M. Hutchings, *Tribology: Friction and Wear of Engineering Materials* (CRC Press, London, 1992).

[14] M.A. Nicholls, T. Do, P.R. Norton, M. Kasrai and G.M. Bancroft, *Tribol. Int.* 38 (2005) 15.
[15] M.L. Suominen Fuller, M. Kasrai and G.M. Bancroft, in: *Chemical Applications of Synchrotron Radiation*, Vol. 12B, ed. T.-K. Sham (World Scientific, New Jersey, 2002) p. 1091.
[16] G.C. Smith, J. Phys. D: Appl. Phys. 33 (2000) R187.
[17] A.M. Barnes, K.D. Bartle and V.R.A. Thibon, Tribol. Int. 34 (2001) 389.
[18] H. Spikes, Tribol. Lett. 17 (2004) 469.
[19] J.M. Martin, C. Grossiord, K. Varlot, B. Vacher and J. Igarashi, Tribol. Lett. 8 (2000) 193.
[20] K. Varlot, J.M. Martin, C. Grossiord, R. Vargiolu, B. Vacher and K. Inoue, Tribol. Lett. 6 (1999) 181.
[21] P.A. Willermet, R.O. Carter III and E.N. Boulos, Tribol. Int. 25 (1992) 371.
[22] M.A. Nicholls, G.M. Bancroft, P.R. Norton, M. Kasrai, G. De Stasio, B.H. Frazer and L.M. Wiese, Tribol. Lett. 17 (2004) 245.
[23] J.F. Graham, C. McCague and P.R. Norton, Tribol. Lett. 6 (1999) 149.
[24] S. Bec, A. Tonck, J.M. Georges, R.C. Coy, J.C. Bell and G.W. Roper, Proc. Roy. Soc. Lond. A 455 (1999) 4181.
[25] A. Tonck, S. Bec, J.M. Georges, R.C. Coy, J.C. Bell and G.W. Roper, in: *Tribology Series: Lubrication at the Frontier*, Vol. 36. ed. D. Dowson (Elsevier Science B.V., Amsterdam, 1999) p. 39.
[26] M. Kasrai, Z. Yin, G.M. Bancroft and K. Tan, J. Vac. Sci. Technol. A 11 (1993) 2694.
[27] K.H. Tan, G.M. Bancroft, L.L. Coatsworth and B.W. Yates, Can. J. Phys. 60 (1982) 131.
[28] T. Tyliszczak, BAN–Data Analysis Program, Unpublished Version 4.64a.
[29] C. Morin, H. Ikeura-Sekiguchi, T. Tyliszczak, R. Cornelius, J.L. Brash, A.P. Hitchcock, A. Scholl, F. Nolting, G. Appel, D.A. Winesett, K. Kaznacheyev and H. Ade, J. Elect. Spectro. Rel. Phen. 121 (2001) 203.
[30] L.M. Croll, J.F. Britten, C. Morin, A.P. Hitchcock and H.D.H. Stoever, J. Synchro. Rad. 10 (2003) 265.
[31] C. Jacobsen, S. Wirick, G. Flynn and C. Zimba, J. Microsc. 197 (2000) 173.
[32] X. Zhang, R. Balhorn, J. Mazrimas and J. Kirz, J. Struct. Bio. 116 (1996) 335.
[33] G. De Stasio, B.H. Frazer, B. Gilbert, K.L. Richter and J.W. Valley, Ultramicroscopy 98 (2003) 57.
[34] A. Scholl, Curr. Opin. Sol. State. Mat. Sci. 7 (2003) 59.
[35] M. Labrenz, G.K. Druschel, T. Thomsen-Ebert, B. Gilbert, S.A. Welch, K.M. Kemner, G.A. Logan, R.E. Summons, G. De Stasio, P.L. Bond, B. Lai, S.D. Kelly and J.F. Banfield, Science 290 (2000) 1744.
[36] G. De Stasio, B. Gilbert, B.H. Frazer, K.H. Nealson, P.G. Conrad, V. Livi, M. Labrenz and J.F. Banfield, J. Elect. Spectro. Rel. Phen. 114–116 (2001) 997.
[37] M. Kasrai, W.N. Lennard, R.W. Brunner, G.M. Bancroft, J.A. Bardwell and K.H. Tan, Appl. Surf. Sci. 99 (1996) 303.
[38] J. Stohr and S. Anders, IBM J. Res. Develop. 44 (2000) 535.
[39] B.H. Frazer, B. Gilbert, B.R. Sonderegger and G. De Stasio, Surf. Sci. 537 (2003) 161.
[40] B.H. Frazer, M. Girasole, L.M. Wiese, T. Franz and G. De Stasio, Ultramicroscopy 99 (2003) 87.
[41] A.P. Hitchcock, P. Hitchcock, C. Jacobsen, C. Zimba, B. Loo, E. Rotenberg, J. Denlinger and R. Kneedler aXis2000 – program available from http://unicorn.mcmaster.ca/aXis2000.html (1997).
[42] I.N. Koprinarov, A.P. Hitchcock, C.T. McCrory and R.F. Childs, J. Phys. Chem. B. 106 (2002) 5358.
[43] O.L. Warren, J.F. Graham, P.R. Norton, J.E. Houston and T.A. Michalske, Tribol. Lett. 4 (1998) 189.
[44] A.J. Pidduck and G.C. Smith, Wear 212 (1997) 254.
[45] M.A. Nicholls, T. Do, P.R. Norton, G.M. Bancroft, M. Kasrai, T.W. Capehart, Y.-T. Cheng and T. Perry, Tribol. Lett. 15 (2003) 241.
[46] Z. Yin, M. Kasrai, M. Fuller, G.M. Bancroft, K. Fyfe and K.H. Tan, Wear 202 (1997) 172.
[47] M. Kasrai, Z. Yin, G.M. Bancroft, K.F. Laycock, K.H. Tan and X. Feng, in: *The 4th European Academy Surface Technology (EAST)-Kongress*, (1993).
[48] T. Tyliszczak, BGAUSS – Multiline Fitting Program, Unpublished Version 2.3 (1994).
[49] Z. Yin, M. Kasrai, G.M. Bancroft, K.H. Tan and X. Feng, Phys. Rev. B 51 (1995) 742.
[50] M. Kasrai, M. Fuller, M. Scaini, Z. Yin, R.W. Brunner, G.M. Bancroft, M.E. Fleet, K. Fyfe and K.H. Tan, in: *Lubricants and Lubrication: Lubrication at the Frontier*, Vol. 30. eds. D. Dowson et al. (Elsevier Science B. V., Amsterdam, 1995). p. 659.
[51] B. Gilbert, G. Margaritondo, S. Douglas, K.H. Nealson, R.F. Egerton, G.F. Rempfer and G. De Stasio, J. Elect. Spectro. Rel. Phen. 114(116) (2001) 1005.
[52] K. Masenelli-Varlot, M. Kasrai, G.M. Bancroft, G. De Stasio B. Gilbert, E.S. Yamaguchi and P.R. Ryason, Tribol. Lett. 14 (2003) 157.
[53] M.A. Hayat, *Principles and Techniques of Scanning Electron Microscopy: Biological Applications* 3(Van Nostrand Reinhold Company, London, 1975).
[54] M.A. Nicholls, G.M. Bancroft, M. Kasrai, P.R. Norton, B.H. Frazer and G. De Stasio (In Preparation).